MATL-DC: A Multi-domain Aggregation Transfer Learning Framework for EEG Emotion Recognition with Domain-Class Prototype under Unseen Targets

Guangli Li[a,1], Canbiao Wu[a,2], Zhehao Zhou[a,3], Na Tian[a,4], Zhen Liang[b,c,5]

[a]School of Biological Science and Medical Engineering, Hunan University of Technology, Zhuzhou, China
[b]School of Biomedical Engineering, Health Science Center, Shenzhen University, Shenzhen, China
[c]Guangdong Provincial Key Laboratory of Biomedical Measurements and Ultrasound Imaging, Shenzhen, China

Email: [1]guangli010@hut.edu.cn, [2]wucanbiao@m.scnu.edu.cn, [3]463805331@qq.com, [4]tiann7@mail2.sysu.edu.cn, [5]Address Correspondence To: janezliang@szu.edu.cn.

***Abstract*— Emotion recognition based on electroencephalography (EEG) signals is increasingly becoming a key research hotspot in affective Brain-Computer Interfaces (aBCIs), and its core goal is accurate decoding and feature alignment of EEG signals. However, the current transfer learning model greatly depends on the source domain and target domain data, and emotion label noise hinder the practical application of emotion recognition. Therefore, we propose a Multi-domain Aggregation Transfer Learning framework for EEG emotion recognition with Domain-Class prototype under unseen targets (MATL-DC). We design the feature decoupling module to decouple class-invariant domain features from domain-invariant class features from shallow features. In the model training stage, the multi-domain aggregation mechanism based on the Maximum Mean Discrepancy (MMD) aggregates the domain feature space to form a superdomain, and extracts the domain prototype representation, which enhances the characteristics of emotional EEG signals. In each superdomain, we further extract the class prototype representation by class features. In addition, we adopt the pairwise learning strategy to transform the sample classification problem into the similarity problem between sample pairs, which effectively alleviates the influence of unavoidable label noise. It is worth noting that the target domain is completely unseen during the training process. In the inference stage, we use the trained domain prototypes and class prototypes for inference, and then realize emotion recognition. We rigorously validate it on the publicly available databases (SEED, SEED-IV and SEED-V). The results show that the accuracy of MATL-DC model is 84.70%, 68.11% and 61.08%, respectively. MATL-DC achieves comparable or even better performance than methods that rely on both source and target domains. Our work provides a promising solution for emotion recognition in unseen target domains. The source code is available at https://github.com/WuCB-BCI/MATL-DC.**

***Index Terms*—EEG; Emotion Recognition; Prototype Representation; Transfer Learning; Unseen Target.**

I. Introduction

EMOTION is a mental state, which is a complex physiological and psychological reaction of human beings to external stimuli or internal activities [1]. It not only affects people's emotions, thinking, and behavior, but also impacts their physical and mental health [2]. Therefore, how to accurately describe and effectively recognize emotional states is an urgent problem to be solved. Affective computing is a rapidly developing interdisciplinary research field, and emotional state recognition is the key content of affective computing. In previous studies, emotion recognition has primarily relied on external cues, such as voice [3], facial expressions [4], and body movements [5], as well as internal physiological signals, including electrocardiography (ECG) [6] and electroencephalography (EEG) [7]. Compared with external cues, emotion recognition based on physiological signals (EEG) has the characteristics of being difficult to disguise, having excellent real-time performance and strong objectivity. It has received increasing attention from researchers in different fields such as computer science, neuroscience, psychology [8] [9].

Currently, deep transfer learning methods have achieved great success in the field of emotion recognition [10]. As shown in Fig.1, transfer learning strategy divide data into source domain (labeled data with known distribution) and target domain (unlabeled data with unknown distribution), and transfer the knowledge and features learned in the source domain to the learning process of the target domain. One of the key challenges of EEG-based deep transfer learning methods is to alleviate individual variability [11]–[15] and improve feature-invariant representations [16]–[18]. For example: Yang *et al*. [19] proposed spectral-spatial attention alignment multi-source domain adaptation (S^2A^2-MSD), which constructs domain attention to represent affective cognition attributes in spatial and spectral domains and utilizes domain consistent loss to align them between domains, and further learning abundant domain-invariant features. Chen *et al*. [20] propose the multi-source marginal distribution adaptation (MS-MDA) for EEG emotion recognition, which takes both domain-invariant and domain-specific features into consideration. MS-MDA is used to solve the limitation that multiple EEG data as a single source domain fails to satisfy the assumption of domain adaptation that the source has a certain marginal distribution. Zhao *et al*. [21] proposed a plug-and-play domain adaptation (PPDA) method for dealing with the inter-subject variability. PPDA method divide EEG representations into private components specific to each subject and shared emotional components that are universal to all subjects, which reduces the model's dependence on large amounts of EEG data.

However, **(1)** the transfer learning paradigm is based on the assumption of model parameter transferability, which believes that there is potential reuse value of network architecture between different tasks, and cross-domain knowledge transfer is realized through parameter transfer or structure sharing. However, this needs to simultaneous rely on the data of the source domain and the target domain at the same time, which means that the model needs to be retrained when it is applied to a new subject, which greatly increases the cost of model training. In addition, the model is also prone to being affected by the data preferences of the target domain, resulting in inflated performance. **(2)** Previous studies have highlighted that EEG signals are highly subject dependent, with significant differences in Emotion perception and affective expression across individuals [22] [23]. These differences are further reflected in the neural mechanisms involved in emotion regulation, increasing the complexity of the emotion recognition task. Furthermore, we highlighting the need to develop innovative methods that adapt to diverse individual EEG patterns while maintaining stable performance. **(3)** Currently, EEG emotion experiments are basically induced by video. Individuals may have different subjective feelings for the same emotional stimulus, and their physiological arousal patterns often show low correlation with self-reports, which brings inevitable label noise to emotion labeling. Traditional pointwise learning strategies usually transform a single sample into a multi-class classification problem in the classification task. Compared with pointwise learning, the pairwise learning strategy can model the correlation between samples, which is less dependent on labels and has better robustness [24] [25].

Therefore, to address the aforementioned triple challenge of data dependence, individual differences and label noise interference, we proposed Multi-domain Aggregation Transfer Learning framework for EEG emotion recognition with Domain and Class prototype (MATL-DC). First, we designed a feature decoupling module to separate domain features (representing individual differences in subjects) and class features (representing emotional commonalities across subjects). Then, Maximum Mean Difference (MMD) was introduced to quantify the discrepancy of feature distribution among subjects to realize the multi-domain aggregation mechanism and form superdomains, which fully exploits the potential distribution commonality among the subject groups while preserving the individual specificity, so that the MATL-DC model can enhance the generalization ability across subjects by using the shared features in the superdomains. Furthermore, we proposed a prototype representation adaptive update mechanism to adaptively fuse the domain class prototype information of historical training cycles. Finally, to reduce the effect of label noise, classification is described as a pairwise learning task. It is noteworthy that the target domain is completely unseen in the training process, which breaks through the dependence of traditional deep transfer learning on target domain data. Overall, the main contributions of this paper are summarized as follows:

- We proposed a Multi-domain Aggregation Transfer Learning framework for EEG emotion recognition with Domain-Class prototype (MATL-DC), which separates domain and class features from shallow features, and the individual variability of EEG signals is conceptualized as a feature shift resulting from the interaction between these features.
- We designed a Multi-Domain Aggregation mechanism to aggregate the domain feature space, and further adopt an adaptive prototype update method to compute domain prototype and class prototype representations, which represent the basic properties of class-invariant domain features and domain-invariant class features.
- We use three publicly available databases (SEED, SEED-IV and SEED-V) for rigorous cross-subject validation. The results show that even though the target domain is unseen, MATL-DC still achieves comparable or even better performance than deep transfer learning models that rely on target domain data. In addition, we thoroughly analyze the model's parameters and feature visualizations to deepen our understanding of the model and results.

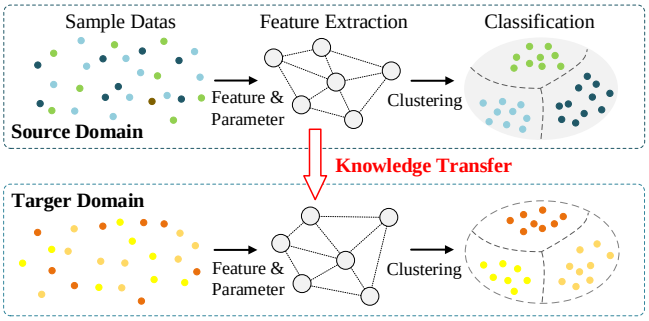

Fig. 1: A simple framework for transfer learning strategies. Transfer learning aims to extract knowledge from one or more source domain and applies the knowledge to a target domain.

The rest of this article is arranged as follows: We briefly described the background to the model in Sec.II. Then in Sec.III, we introduce the concrete implementation of our proposed MATL-DC in detail. Our experimental results was described in Sec.IV. Finally, We discuss our model performance and conclusions in Sec.V.

II. Related Work

A. Non-Deep-Learning-Based Emotion Recognition

In the early research on emotion recognition, researchers mainly relied on non-deep learning methods to extract emotional EEG features and recognize different emotions [26]. These studies have yielded valuable insights and paved the way for the development of affective brain-computer interface (aBCI) systems. For example:

Wang *et al*. [27] proposed the minimum redundancy maximum relevance (MRMR) method to extract common critical features across subjects, and introduces an emotion recognition system based on EEG signals. The results show that the emotional state can be recognized by using frequency domain features and support vector machine (SVM). Duan *et al*. [28] proposed a new effective EEG feature named differential

entropy (DE) to represent the characteristics associated with emotional states, and further confirmed that DE is more suitable for emotion recognition than the traditional feature. It is also confirmed that EEG signals on frequency band Gamma relates to emotional states more closely than other frequency bands. Mohammadi *et al*. [29] proposed a method for classifying human emotions using machine learning models and extracting discrete wavelet features from EEG signals, and considered a significant band of EEG with a reduced frontal electrode to get a better results. Liu *et al*. [30] proposed a novel emotional EEG feature extraction method: kernel Eigen-emotion pattern (KEEP), And an adaptive SVM is also proposed to deal with the learning problem in imbalanced emotional EEG datasets. Results show that KEEP gives much better classification results than the widely-used EEG frequency band power features.

B. Deep Transfer Learning Based Emotion Recognition

In recent years, with the progress of deep learning theory and technology, a large number of transfer algorithms based on deep learning have been introduced to enhance the performance and generalization ability of the model, and have been widely used in the field of EEG-based aBCI [31].

Zhou *et al*. [32] proposed an EEG-based Emotion Style Transfer Network (E2STN) to obtain EEG representations that contain the content information of source domain and the style information of target domain, which is called stylized emotional EEG representations, and this representations are helpful for discriminative prediction. Li *et al*. [33] proposed a novel neural network model, called bi-hemisphere domain adversarial neural network (BiDANN) model, for EEG emotion recognition. It contains a global and two local domain discriminators that work adversarially with a classifier to learn discriminative emotional features for each hemisphere. He *et al*. [34] proposed a novel domain adaptation strategy called adversarial discriminative-temporal convolutional networks (AD-TCNs), which can ensure the invariance of the representation of feature graphs in different domains and fill in the differences between different domains. Li *et al*. [35] proposed a joint domain adaptation network, which are optimized by minimizing the classification error on the source while making the source and the target similar in their latent representations. Luo *et al*. [36] proposed a novel Wasserstein generative adversarial network domain adaptation (WGANDA) framework for building cross-subject EEG-based emotion recognition models. The proposed framework consists of GANs-like components and a two-step training procedure with pre-training and adversarial training.

C. Prototype Learning

The core concept of prototype learning is that each class is represented by a prototype representation (a feature vectors with representative features), and the task recognition is performed by evaluating the proximity or similarity between the sample features and the prototype representation [37].

Wang *et al*. [38] incorporated an efficient prototype-based data representation to learn a more discriminative embedded feature space for EEG-based emotion recognition, in which the Euclidean metric was adopted to assess the associations between the data samples and all the selected prototypes. Zhou *et al*. [39] proposed a novel transfer learning framework with Prototypical Representation based Pairwise Learning (PR-PL). The discriminative and generalized EEG features are learned for emotion revealing across individuals and the emotion recognition task is formulated as pairwise learning for improving the model tolerance to the noisy labels. Wang *et al*. [40] proposed a prototype-based domain adaptation SPD matrix network (daSPDnet) that can successfully capture an intrinsic emotional representation shared between different subjects, which jointly exploits feature adaptation with distribution confusion and sample adaptation with centroid alignment. Guo *et al*. [41] proposed and implement a novel neural network algorithm based on modifying the emotional neural network (EmNN) model to unify the prototype- and adaptive-learning theories, as well as apply the proposed model to two real-life challenging emotion tasks, static hand-gesture recognition and face recognition.

However, the current most emotion recognition models need to rely on both source domain and target domain data, which greatly increases the practical application cost, and the robustness and generalization ability are limited. Therefore, the model framework based on unseen target domains emphasizes the importance of its development.

TABLE I: Frequently used notations and descriptions.

Notation	*Description*
$\mathbb{S}/\mathbb{T}$	Source/Target Domain
x_d/x_c	Domain/Class Feature
y_d/y_c	Domain/Class Label
$f_g(\cdot)$	Shallow Feature Extractor
$f_d(\cdot)/f_c(\cdot)$	Domain/Class Feature Decoupler
$D_d(\cdot)/D_c(\cdot)$	Domain / Class Discriminator
μ_d/μ_c	Domain / Class Prototype Representation
$R(\cdot)$	Gradient Reversal Layer
$\mathcal{HK}$	Reproducing Kernel Hillbert Space
K	Number of Superdomains
θ	Bilinear Transformation Matrix
ψ	Domain Distribution

III. METHODOLOGY

Inspired by previous research [42]–[44], we assume that EEG features involve two types of deep features: domain-invariant class features and class-invariant domain features. Domain-invariant class features capture the semantic information of the emotion category to which the sample belongs, while domain-invariant class features express the specific information generated by the individual differences of the subjects. The distribution differences of EEG signals among different subjects can be attributed to the variation of domain features, which leads to the dispersion of class feature distribution. Based on the above assumptions, We regard the original EEG features as the fusion of these two features. Therefore, we extracts EEG features while considering both domain-specific and class-specific components to enhance robustness

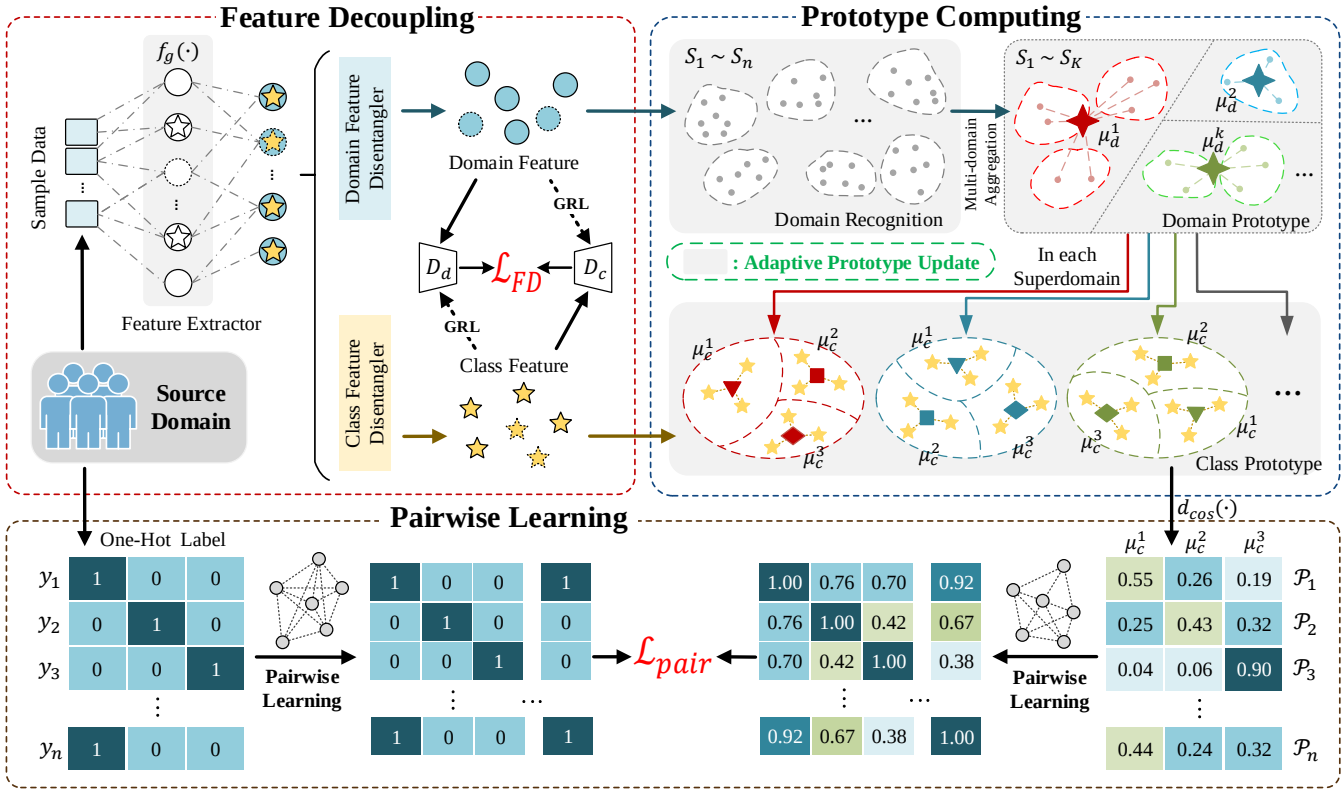

Fig. 2: The training phase of the MATL-DC framework. MATL-DC consists of three main modules, which are feature decoupling module, prototype computing module and pairwise learning module. The goal of model training is to obtain optimal parameters for domain prototype and class prototype representations. Here, D_d and D_c represent Domain discriminator and Class discriminator, respectively. GRL represent Gradient Reversal Layer. $S_1 \sim S_n$ represent the domain space. $S_1 \sim S_K$ represent the aggregated superdomain space. μ_d denotes the domain prototype representation of the superdomain. μ_c denotes the class prototype representation within each superdomain space. $d_{cos}(\cdot)$ represents the cosine similarity calculation, which is used to evaluate the relationship between class features and class prototypes.

and generalization capabilities across subjects.

Suppose the source domain and the target domain are represented as $(\mathbb{S}, \mathbb{T})$. In the source domain, we define the sample distribution of each subject as an independent domain. Each subject has a domain space, so the source domain is composed of multiple domain Spaces. The source domain is defined as $\mathbb{S} = \{S_n\}_{n=1}^{N_d}$, where N_d represents the number of subjects in the source domain. EEG samples for each of the subjects, defined as $S_n = \{x_n^i, y_n^i\}_{i=1}^{N_s}$, where x_n^i represents the i_{th} sample data of the n_{th} subject, y_n^i is the corresponding emotion label, and N_s indicates the sample capacity of the n_{th} subject in the source domain. Target domain sample defined as $\mathbb{T} = \{x_t^i, y_t^i\}_{i=1}^{N_t}$, where N_t represents the target domain of EEG sample capacity. The target domain is completely unseen during training. For ease of inquiry, common notations and descriptions are displayed in TABLE I.

A. Feature Decoupling

As shown in Fig.2, assuming that the shallow feature extractor $f_g(\cdot)$ is used to extract the shallow features of the sample, we introduce a domain feature decoupler $f_d(\cdot)$ and a class feature decoupler $f_c(\cdot)$ to decouple the semantic information in these shallow features, thereby obtaining the class-invariant domain features $x_d = f_d(f_g(x))$ and domain-invariant class features $x_c = f_c(f_g(x))$, respectively. To ensure that the feature decoupler can accurately separate two types of features, we utilize a domain discriminator $D_d(\cdot)$ and a class discriminator $D_c(\cdot)$ to identify the domain or category to which the features belong. Specifically, our goal is to enable the domain discriminator to accurately identify the domain to which the domain features belong, rather than using the domain features to identify the category to which they belong. On the contrary, the class discriminator can accurately identify the category to which the class feature belongs, but cannot use the class feature to identify the domain to which it belongs. By employing a decoupler and discriminator through adversarial training for successful decoupling of domain-specific and class-specific characteristics.

To achieve this goal, we perform adversarial training of the decoupler and discriminator. Before the class-specific features are fed into the domain discriminator and the domain-specific features are fed into the class discriminator, we pass through a Gradient Reversal Layer (GRL) to facilitate adversarial training. Specifically, the model maintains the input features unchanged during forward propagation, where data flows directly fed the network. During backpropagation, the GRL

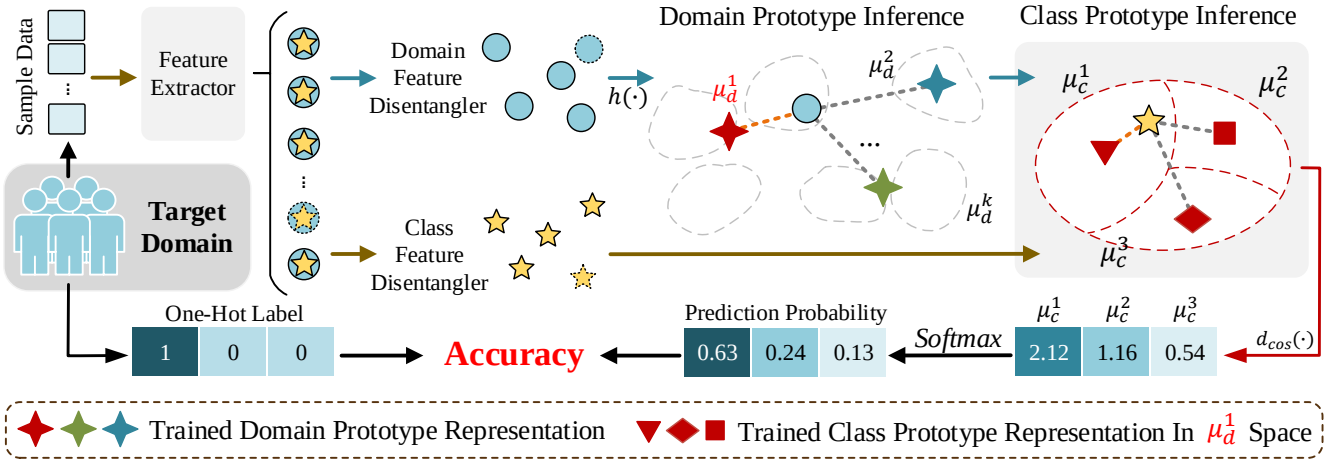

Fig. 3: The inferencding phase of the MATL-DC framework. The optimal domain prototype μ_d and class prototype μ_c obtained during the model training phase are transferred to the target domain inference. For example, after feature separation, the model determines the superdomain μ_d^1 to which the sample belongs by Domain Prototype Inference, and within this superdomain, we perform Class Prototype Inference to determine the category μ_c^1 to which the sample belongs. Here, $h(\cdot)$ represent the bilinear transformation to capture the most relevant domain space (Eq.13). $d_{cos}(\cdot)$ represents the cosine similarity calculation (Eq.15).

multiplies the gradients by a negative coefficient, reversing their direction to enable adversarial training. We use the Binary Cross-Entropy (BCE) loss function to optimize the discriminator, converting the multi-class problem into several independent binary classification tasks. Suppose the GRL layer is represented by $R(\cdot)$, x_d and x_c represent domain features and class features, respectively, then the class discriminator loss function $\mathcal{L}_{cls}$ is defined as:

$$\mathcal{L}_{cls} = \ell_{BCE}[D_c(x_c), y_c] + \ell_{BCE}[D_c(R(x_d)), y_c] \quad (1)$$

here, $\ell_{BCE}(\cdot)$ represents the BCE loss function, y_c represents the true label of the class feature. Similarly, the domain discriminator loss function $\mathcal{L}_{dom}$ is defined as:

$$\mathcal{L}_{dom} = \ell_{BCE}[D_d(x_d), y_d] + \ell_{BCE}[D_d(R(x_c)), y_d] \quad (2)$$

Therefore, the objective function $\mathcal{L}_{FD}$ of the feature decoupling module is defined as:

$$\mathcal{L}_{FD} = \mathcal{L}_{cls} + \mathcal{L}_{dom} \quad (3)$$

B. Multi-Domain Aggregation

We defined the distribution of each subject sample as an independent domain. In the feature decoupling module, the domain discriminator identifies multiple domain ($S_{1:n}$) based on the number of subjects. However, we argue that EEG samples from different subjects may not be exclusively associated with a single domain, but rather exhibit latent connections to multiple domains. Furthermore, as the scale of the subjects expands, too many domains will lead to a significant increase in computational costs, thereby reducing the operational and response efficiency of the model. Therefore, we need to aggregate the domains with potential connections to form a superdomain.

Specifically, we need to quantify the discrepancy between the domain feature distributions of different domains for multi-domain aggregation. To achieve this goal, we adopt the Maximum Mean Discrepancy (MMD) strategy as the discrepancy measure. MMD is a non-parametric kernel method for measuring the discrepancy between two probability distributions, which can implicitly capture complex discrepancy in high-dimensional feature Spaces. Suppose two independent sample sets, X and Y, follow the P and Q distribution respectively ($X \sim P, Y \sim Q$), the MMD is defined as:

$$MMD^2_{\mathcal{HK}}(P, Q) = \left\| \mathbb{E}_x \left[\phi(X) \right] - \mathbb{E}_y \left[\phi(Y) \right] \right\|^2_{\mathcal{HK}} \quad (4)$$

here, $\mathbb{E}_x$ and $\mathbb{E}_y$ represent the Mathematical Expectation of X and Y, respectively. $\mathcal{HK}$ denote the Reproducing Kernel Hilbert Space (RKHS) mapped by the feature kernel κ, and $\phi(\cdot)$ represents this mapping operation. The feature kernel κ can be interpreted as the distance function, which defines the distance measure between X and Y in the RKHS. This distance measure can be obtained by computing the inner-product of samples, assume domain samples are denoted as $X = \{x_i\}_{i=1}^n$ and $Y = \{y_j\}_{j=1}^m$, denoted as $\kappa(x, y) = \langle \phi(x), \phi(y) \rangle$. Due to the non-stationary characteristics and high-dimensional spatio-temporal characteristics of EEG signals, we introduce Gaussian-Kernel function (GKF) to replace the traditional linear kernel function. GKF can map the data into an RKHS of infinite-dimensions to obtain the inner-product result without explicitly computing the mapping function $\phi(\cdot)$. GKF is define as:

$$\kappa(x, y) = \exp\left(-\frac{\|x - y\|^2}{2\sigma^2} \right) \quad (5)$$

here, $\|\cdot\|^2$ denotes the L2 norm. σ represent the bandwidth parameter. Therefore, Eq.4 can be transformed using GKF as:

$$\begin{aligned} MMD^2_{\mathcal{HK}}(X,Y) &= \frac{1}{n(n-1)}\sum_{i=1}^{n}\sum_{j=1}^{n}\kappa(x_i,x_j) \\ +\frac{1}{m(m-1)}\sum_{i=1}^{m}\sum_{j=1}^{m}\kappa(y_i,y_j) &- \frac{2}{nm}\sum_{i=1}^{n}\sum_{j=1}^{m}\kappa(x_i,y_j) \end{aligned} \tag{6}$$

The model is iteratively optimized, and obtained the MMD distance between each domain and all other domains, and form an MMD distance vector, which provides distance reference for multi-domain aggregation. In summary, the distance vector for the i_{th} domain is defined as:

$$\mathcal{V}_i = [MMD^2_{i,1}, MMD^2_{i,2}, \cdots, MMD^2_{i,N}] \tag{7}$$

here, N represents the number of domains in the source domain. The coordinate positions of $\mathcal{V}_i$ reflect the distribution characteristics of this domain. Next, we perform multi-domain aggregation based $\mathcal{V}$ to form a certain number of superdomains.

K-means++ is a traditional clustering algorithm, which clusters by calculating the Euclidean distance between samples, and can avoid the extreme situation that the clustering centroid is too concentrated. Considering the characteristics of EEG signals and the aggregation performance of EEG data in the feature space, we innovated to use MMD distance to replace the traditional Euclidean distance in the K-means++, and formed a new K-means++ algorithm based on MMD. As shown in Fig.2, a superdomain is aggregated from multiple domains. Assuming the superdomain defined as S_k, the clustering algorithm is defined as:

$$\mathcal{J} = \sum_{k=1}^{K}\sum_{(X/Y)\in S_k} MMD^2\left(X,Y\right) \tag{8}$$

here, K denotes the number of superdomains. Eventually, we repartition the source domain into $\mathbb{S} = [\mathcal{S}_1, \mathcal{S}_2, \cdots, \mathcal{S}_K]$.

C. Adaptive Prototype Updating

For each superdomain, we assume the existence of a domain prototype representation, which embodies the essential characteristics of the domain features belonging to that superdomain. Samples within the same superdomain are distributed around prototype representation. From the perspective of probability distributions, the prototype representation can be regarded as the centroid of all domain features in superdomain. Similarly, within each superdomain, features corresponding to different emotional states can derive class prototype representations. The class prototype representation capture the fundamental attributes of each EEG emotion state in the superdomain. Therefore, extracting domain & class prototype representation can improve the robustness and generalization performance of the model. Assume that the domain feature and superdomain label in the superdomain S_k are represented as $\{x^i_d, k\}_{i=1}^{|X^k_d|}$, $|X^k_d|$ denotes the number of domain features in the superdomain. Therefore, the domain prototype representation is defined as:

$$\mu^k_d = \frac{1}{|X^k_d|}\sum_{x^i_d \in X^k_d} x^i_d \tag{9}$$

Similarly, in each superdomain space, the class features and labels are denoted as $\{x^i_c, m\}_{i=1}^{|X^m_c|}$, and $|X^m_c|$ is denoted as the number of class features belonging to category m. Thus, the class prototype representation within each superdomain space are defined as:

$$\mu^m_c = \frac{1}{|X^m_c|}\sum_{x^i_c \in X^m_c} x^i_c \tag{10}$$

During the training phase, As shown in the Prototype Computing module of Fig.2, domain prototypes and class prototype representations are continuously updated through iterations to seek optimal parameter. However, in the process of model iteration, the obtained prototype representation may have large deviation even for two adjacent training moments. To avoid the possible instability of prototype calculation at different moments, we adopt an adaptive prototype update mechanism, and the prototype representation calculation at time t is affected by the time $t-1$, so as to improve the stability of model training. The update process is defined as:

$$\begin{aligned} \mu^{(t)}_d &= (1-\alpha)\mu^{(t-1)}_d + \alpha\mu^{(t)}_d \\ \mu^{(t)}_c &= (1-\alpha)\mu^{(t-1)}_c + \alpha\mu^{(t)}_c \end{aligned} \tag{11}$$

here, α is the weight update parameter. In the early stage of training, the feature distribution changes drastically, and the prototype representation needs to be updated quickly to adapt to this dynamic adjustment. In the later stage of training, as the model tends to converge and the feature distribution tends to be stable, the update rate of the prototype should slow down. Thus, α is defined as:

$$\alpha = \alpha_l + (\alpha_h - \alpha_l)\left(1 - \frac{t}{maxEpoch}\right)^p \tag{12}$$

here, α_h and α_l represent the upper and lower threshold of α, respectively. p is the hyperparameter that controls the rate of decay. When $p > 1$, α will decay rapidly at the beginning, and as the model continues to train, the decay rate will gradually slow down until we reach our desired goal.

D. Prototype Inference

In the training phase, MATL-DC model obtains the optimal domain prototype and the class prototype in each superdomain space by the adaptive update method. It is worth noting that the MATL-DC is completely unseen to the target domain samples during training. As shown in Eq.3, in the model inference stage, we first extract the corresponding domain features and class features in target domain. Next, we perform domain prototype inference to determine the superdomain space by trained domain prototype representation. Then, in the selected superdomain space, class prototype inference is performed through the trained class prototypes to determine the emotional state labels. Specifically, we introduce a bilinear

transformation to quantify the interaction between domain features x_d and the domain prototype μ_d^k. Assume that the bilinear transformation expressed as $h(\cdot)$, which is defined as:

$$h(x_d, \mu_d^k) = (x_d)^T \cdot \theta \cdot \mu_d^k \tag{13}$$

here, $(\cdot)^T$ denotes the transpose operation. θ is a trainable, randomly initialized bilinear transformation matrix that is not limited by positive definiteness or symmetry. θ is beneficial to enhance the feature representation ability. Overall, the interaction between x_d and all superdomains $\mu_d^k (k = 1 : K)$ are represented as a vector, and the coordinate with the highest value corresponds to the superdomain to which it belongs, which is defined as:

$$\mathcal{V}_i = softmax\left[h(x_d^i, \mu_d^1), \cdots, h(x_d^i, \mu_d^K)\right] \tag{14}$$

here, $softmax$ represent normalization function. Then, in the selected superdomain, we adopt cosine similarity strategy to calculate the similarity between class prototypes $\mu_c^m (m = 1 : M)$ and class features x_c^i of samples. The $\mu_c^m (m = 1 : M)$ and x_c^i form an interaction relationship to determine the class to which the sample belongs, which is defined as:

$$\mathcal{P}_i = softmax\left[d_{cos}(x_c^i, \mu_c^1), \cdots, d_{cos}(x_c^i, \mu_c^M)\right] \tag{15}$$

here, $d_{cos}(\cdot)$ represents the cosine similarity calculation, and the coordinate with the highest similarity is the emotional state category.

E. Pairwise Learning

We adopt a pairwise learning strategy instead of the traditional pointwise learning to solve the problem of label noise and enhance the resistance of the model to label noise. Unlike pointwise learning, pairwise learning focuses on the latent relationship between samples and captures the relative association between them. Specifically, we transform the classification problem of samples into a similarity problem between samples. The pairwise learning loss function is defined as follows.

$$\mathcal{L}_{pair} = \frac{1}{(N_b)^2} \cdot \sum_{i,j \in N_b} \left[r_{ij} \log\left(\mathcal{G}(x_c^i, x_c^j)\right) - (1 - r_{ij}) \log\left(1 - \mathcal{G}(x_c^i, x_c^j)\right)\right] \tag{16}$$

here, N_b represents the number of samples in each batch during model training. r_{ij} indicates whether the samples x_i and x_j belong to the same emotion category, and the value is 0 or 1. $r_{ij} = 1$ indicates that the sample pairs belongs to the same emotion category, and $r_{ij} = 0$ indicates that they do not belong to the same emotion category. $\mathcal{G}(\cdot)$ represents the similarity measure between samples pair, which is also the probability that samples x_i and x_j belong to the same emotion category. The value of $\mathcal{G}(\cdot)$ ranges from 0 to 1. The closer the value is to 1, the more likely the sample pair is to belong to the same emotion category, and vice versa. Overall, $\mathcal{G}$ is defined as:

$$\mathcal{G}(x_i, x_j) = \frac{\mathcal{P}_i \cdot \mathcal{P}_j}{\|\mathcal{P}_i\|_2 \, ||\mathcal{P}_j||_2} \tag{17}$$

here, $\mathcal{P}_i$ and $\mathcal{P}_j$ are obtained by Eq.15, and $(\cdot)$ denotes the inner product operation. $|| \cdot ||_2$ denotes the L2 constraint. In addition, to avoid redundant feature extraction, we introduce soft regularization $\mathcal{R}$ with a weight parameter of β. Finally, the objective function of our proposed PL_MDCP framework is defined as:

$$\mathcal{L}_{PL\_MDCP} = \mathcal{L}_{FD} + \mathcal{L}_{pair} + \beta\mathcal{R} \tag{18}$$

IV. Experimental Results

A. Databases and Data Processing

We rigorously validated the proposed MATL-DC framework using three established public databases: SEED [45], SEED-IV [46] and SEED-V [47], which are extensively utilized in affective computing research. The **SEED dataset** comprising 15 subjects, each subject completed 3 experimental sessions on separate dates. Each session contained 15 trials and include 3 emotions: positive, neutral and negative, induced by video clips and simultaneously recorded EEG signals. The **SEED-IV dataset** consists of 15 subjects, each of whom participated in 3 experimental sessions on different dates. Each session consists of 24 trials and contains four emotions: neutral, sad, fear and happy. In the **SEED-V dataset**, a total of 16 subjects participated, and each subject completed 3 sessions. Each session consisted of 15 trials with five emotions: happy, neutral, sad, disgust and fear.

The EEG signals in the database are preprocessed as follows: First, the EEG signals are downsampled to a 200 Hz sampling rate, and noise is manually removed, such as electromyography (EMG) and electrooculography (EOG). The denoised data is then filtered using a bandpass filter with a range of 0.3 Hz to 50 Hz. Second, for each experiment, the signals are segmented using a 1-s window, and differential entropy (DE [48]) features, representing the logarithmic energy spectrum of specific frequency bands, are extracted based on five frequency bands: Delta (1-3 Hz), Theta (4-7 Hz), Alpha (8-12Hz), Beta (14-30Hz), and Gamma (31-50Hz), resulting in 310 features for each EEG segment (5 frequency bands × 62 channels). Finally, a Linear Dynamic System (LDS) is applied to smooth all obtained features, leveraging the temporal dependency of emotional changes to filter out EEG components unrelated to emotions and those contaminated by noise. [49] The EEG processing procedure adheres to the same standards as previous studies to enable fair comparisons with models presented in previous literature.

B. Implementation Results

In the proposed model, the architecture of the shallow feature extractor $f_g(\cdot)$ is designed as: input layer (310) - hidden layer (64) - LeakyRelu activation ($\alpha = 0.01$) - hidden layer (64) -nLeakyRelu activation ($\alpha = 0.01$) - output layer (64). The architecture of the domain/class feature decoupler $f_d(\cdot)/f_c(\cdot)$ are designed as: input layer (64) - hidden layer (64) - Relu activation - hidden layer (64) - Relu activation - output layer (64). The architecture of the domain/class discriminator $D_d(\cdot)/D_c(\cdot)$ are designed as: input layer (64) - hidden layer (64) - Dropout layer($p = 0.25$) - hidden layer

TABLE II: Cross-subject single-session leave-one-subject-out cross-validation results on SEED dataset, expressed as (Mean-Accuracy%±Standard-Deviation%). Here, '*' indicates the results are obtained by our own implementation.

Methods	$P_{acc}(\%)$	Methods	$P_{acc}(\%)$
Traditional machine learning methods			
KNN* [50]	55.26 ± 12.43	KPCA* [51]	48.07 ± 09.97
SVM* [52]	70.62 ± 09.02	SA* [53]	59.73 ± 05.40
TCA* [54]	58.12 ± 09.52	CORAL* [55]	71.48 ± 11.57
GFK* [56]	56.71 ± 12.29	RF* [57]	62.78 ± 06.60
Deep learning methods			
DAN* [58]	82.54 ± 09.25	DANN* [59]	81.57 ± 07.21
DDC* [60]	75.42 ± 10.15	DCORAL* [61]	82.90 ± 06.97
DGCNN [62]	79.95 ± 09.02	MMD [63]	80.88 ± 10.10
BiDANN [33]	83.28 ± 09.60	RGNN [64]	79.00 ± 14.80
EFDMs [65]	78.40 ± 06.76	MS-MDA* [20]	77.65 ± 11.32
MATL-DC			**84.70 ± 04.63**

TABLE III: Cross-subject single-session leave-one-subject-out cross-validation results on SEED-IV dataset, expressed as (Mean-Accuracy%±Standard-Deviation%). Here, '*' indicates the results are obtained by our own implementation.

Methods	$P_{acc}(\%)$	Methods	$P_{acc}(\%)$
Traditional machine learning methods			
KNN* [50]	41.77 ± 09.53	KPCA* [51]	29.25 ± 09.73
SVM* [52]	50.50 ± 12.03	SA* [53]	34.74 ± 05.29
TCA* [54]	44.11 ± 10.76	CORAL* [55]	48.14 ± 10.38
GFK* [56]	43.10 ± 09.77	RF* [57]	52.67 ± 13.85
Deep learning methods			
DAN* [58]	59.27 ± 14.45	DANN* [59]	57.16 ± 12.61
DCORAL* [61]	56.05 ± 15.60	DDC* [60]	58.02 ± 15.14
MS-MDA [20]	61.43 ± 15.71	MMD [63]	59.34 ± 05.48
DGCNN [62]	52.82 ± 09.23	BiDANN [33]	65.59 ± 10.39
MATL-DC			**68.11 ± 11.02**

TABLE IV: Cross-subject single-session leave-one-subject-out cross-validation results on SEED-V dataset, expressed as (Mean-Accuracy%±Standard-Deviation%). Here, '*' indicates the results are obtained by our own implementation.

Methods	$P_{acc}(\%)$	Methods	$P_{acc}(\%)$
Traditional machine learning methods			
KNN* [50]	35.73 ± 07.98	KPCA* [51]	35.47 ± 09.39
SVM* [52]	53.14 ± 10.10	SA* [53]	36.06 ± 11.55
TCA* [54]	37.57 ± 13.47	CORAL* [55]	55.18 ± 07.42
GFK* [56]	38.32 ± 10.11	RF* [57]	42.29 ± 16.02
Deep learning methods			
DAN* [58]	59.36 ± 16.83	DANN* [59]	56.28 ± 16.25
DCORAL* [61]	56.26 ± 14.56	DDC* [60]	56.54 ± 18.35
MATL-DC			**61.08 ± 11.02**

TABLE V: Cross-subject cross-session leave-one-subject-out cross-validation results on SEED dataset, expressed as (Mean-Accuracy%±Standard-Deviation%). Here, '*' indicates the results are obtained by our own implementation.

Methods	$P_{acc}(\%)$	Methods	$P_{acc}(\%)$
Traditional machine learning methods			
KNN* [50]	60.18 ± 08.10	KPCA* [51]	72.56 ± 06.41
SVM* [52]	68.01 ± 07.88	SA* [53]	57.47 ± 10.01
TCA* [54]	63.63 ± 06.40	CORAL* [55]	55.18 ± 07.42
GFK* [56]	60.75 ± 08.32	RF* [57]	72.78 ± 06.60
Deep learning methods			
DAN* [58]	78.12 ± 05.47	DANN* [59]	78.42 ± 07.57
DCORAL* [61]	77.36 ± 06.27	DDC* [60]	73.22 ± 05.48
AdaMatch* [66]	78.14 ± 06.18	EmT-B [67]	78.80 ± 12.00
IAG* [68]	74.36 ± 11.11	AMDET* [69]	72.10 ± 16.80
EmT-S [67]	78.00 ± 11.70	GCB-Net* [70]	68.40 ± 17.20
MATL-DC			**80.21 ± 06.32**

(64) - Sigmoid activation - output layer (64). In the Multi-Domain Aggregation module, we set the number of aggregated superdomains to 4. In Eq.12, the upper/lower thresholdupper (α_h/α_l) of the prototype update weight parameter are set to 0.8/0.2, and the hyperparameter p is set to 2. The β in Eq.18 is set to 0.01. All models are executed under the following configuration: Python=3.8, CUDA=11.8, PyTorch=2.0.0, Numpy=1.24.3, Scikit-learn=0.22.1, NVIDIA GeForce RTX 3090.

C. Experiment Protocols

To thoroughly evaluate the model's performance and enable a comprehensive comparison with existing methods, we adopt two different cross-validation protocols. It is worth noting that the target domain data is completely unseen during the training process of the model. **(1) Cross-Subject Single-Session Leave-One-Subject-Out Cross-Validation**, which is a widely used validation method in EEG-based emotion recognition tasks. In this protocols, one subject's signal sessions' data as the target domain, and the remaining subjects' signal sessions as the source domain. Keeping the same as the other research, only data from the first session were used. We repeat training and validation until each subject is treated as the target domain, and the experimental results are averaged. **(2) Cross-Subject Cross-Session Leave-One-Subject-Out Cross-Validation**. To more closely simulate practical application scenarios, we use one subject's all sessions' data as the target and the remaining subjects' all sessions as the source. We repeat training and validation until each subject is treated as the target domain, and the experimental results are averaged. In the EEG-based emotion recognition task, this evaluation Protocol poses the greatest challenge to the validity of the model.

D. Cross-Subject Single-Session Leave-One-Subject-Out Cross-Validation

We rigorously validate the proposed MATL-DC model and compare it with other state-of-the-art (SOTA) methods. The validation results for the SEED database are shown in TABLE II. The MATL-DC model shows significant performance advantages over traditional machine learning. The MATL-DC model achieves 84.70% accuracy, compared with the best machine learning model CORAL(71.48%), the performance is improved by 13.22%. In addition, MATL-DC still

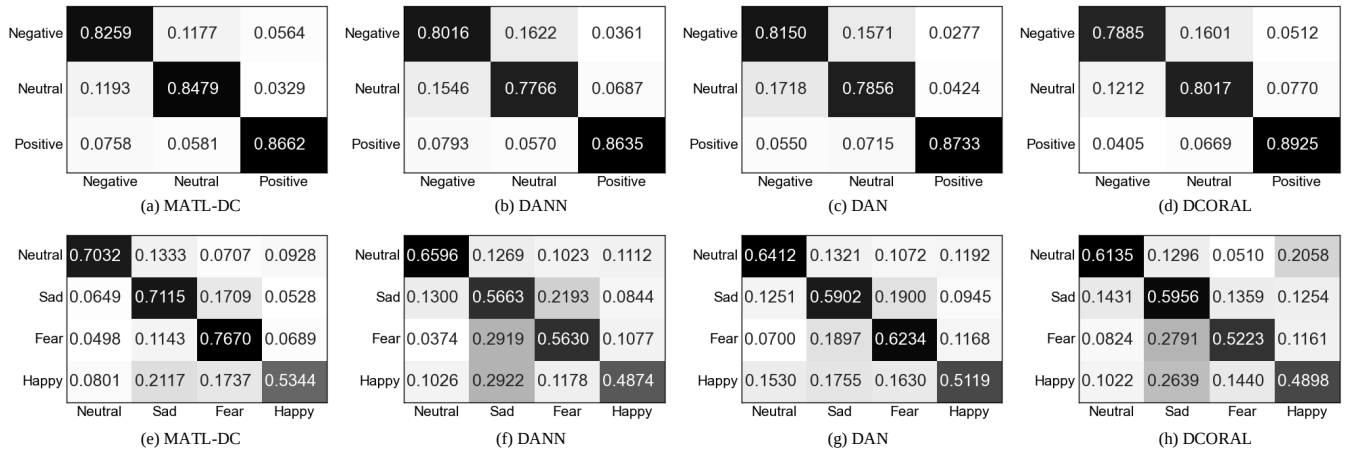

Fig. 4: Confusion matrices of different model settings under cross-subject single-session leave-one-subject-out cross-validation. The SEED database contains three emotion categories: negative, neutral and positive. Among them, (a) MATL-DC; (b) DANN; (c) DAN; (d) DCORAL. the Seed-IV database contains four emotion categories: happy, sad, calm and fear. Among them, (e) MATL-DC; (f) DANN; (g) DAN; (h) DCORAL. The horizontal axis represents the predicted labels, while the vertical axis represents the true labels.

TABLE VI: Cross-subject cross-session leave-one-subject-out cross-validation results on SEED-IV dataset, expressed as (Mean-Accuracy%±Standard-Deviation%). Here, '*' indicates the results are obtained by our own implementation.

Methods	$P_{acc}(\%)$	Methods	$P_{acc}(\%)$
Traditional machine learning methods			
KNN* [50]	40.06 ± 04.98	KPCA* [51]	47.79 ± 07.85
SVM* [52]	48.36 ± 07.51	SA* [53]	40.34 ± 05.85
TCA* [54]	43.01 ± 07.13	CORAL* [55]	50.01 ± 07.93
GFK* [56]	43.48 ± 06.27	RF* [57]	48.16 ± 09.43
Deep learning methods			
DAN* [58]	60.95 ± 09.34	DANN* [59]	61.44 ± 11.66
DCORAL* [61]	59.96 ± 09.03	DDC* [60]	54.76 ± 09.02
GCPL [71]	62.65 ± 09.79	MS-MDA [20]	59.34 ± 05.48
A-LSTM [72]	55.03 ± 09.28	IAG [68]	62.64 ± 10.25
ADAST [73]	53.66 ± 13.63	MFA-LR [74]	61.66 ± 11.53
MATL-DC			**64.51 ± 09.22**

TABLE VII: Cross-subject cross-session leave-one-subject-out cross-validation results on SEED-V dataset, expressed as (Mean-Accuracy%±Standard-Deviation%). Here, '*' indicates the results are obtained by our own implementation.

Methods	$P_{acc}(\%)$	Methods	$P_{acc}(\%)$
Traditional machine learning methods			
KNN* [50]	35.28 ± 07.57	KPCA* [51]	39.68 ± 11.28
SVM* [52]	41.20 ± 10.76	SA* [53]	31.87 ± 09.87
TCA* [54]	37.68 ± 08.40	CORAL* [55]	54.68 ± 07.44
GFK* [56]	37.89 ± 09.84	RF* [57]	43.63 ± 11.38
Deep learning methods			
A-LSTM [72]	40.34 ± 08.68	DANN* [59]	52.83 ± 13.90
DCORAL* [61]	52.23 ± 12.76	DDC* [60]	43.89 ± 11.84
ADAST [73]	50.69 ± 14.01	DAN* [58]	54.27 ± 10.42
MATL-DC			**58.39 ± 08.63**

achieves the SOTA performance compared with other deep learning models. Compared with the sub-optimal performance model DiDANN (83.28%), MATL-DC improved by 1.42%. The results on the SEED-IV dataset are shown in TABLE III. MATL-DC achieves SOTA performance in both machine learning and deep learning methods. RF and BiDANN model achieve sub-optimal performance in machine learning and deep learning methods, with the accuracy of 52.67% and 65.59%, respectively. MATL-DC achieves the accuracy of 68.11%, compared with the sub-optimal model, performance is improved by 15.44% and 2.52%. The results on the SEED-V database are shown in TABLE IV. The MATL-DC model achieves an accuracy of 61.08%, which is better than other model frameworks. Compared with the sub-optimal deep learning model DAN(59.36%), the performance of MATL-DC is improved by 1.72%.

It is worth noting that the target domain data is unseen during training of our proposed model. Other methods use the target domain data in the training process, but MATL-DC still achieves comparable or even slightly better performance than the methods that use the target domain data. These results prove that MATL-DC has strong robustness and generalization ability.

E. Cross-Subject Cross-Session Leave-One-Subject-Out Cross-Validation

Compared with cross-subject single-session, cross-subject cross-session not only considers the differences between subjects, but also integrates the differences between sessions.

The validation results for the SEED database are shown in TABLE V. The accuracy of MATL-DC model reaches 80.21%, which is is significantly better than traditional machine learning methods and deep learning methods. In the machine learning method, compared with the sub-optimal

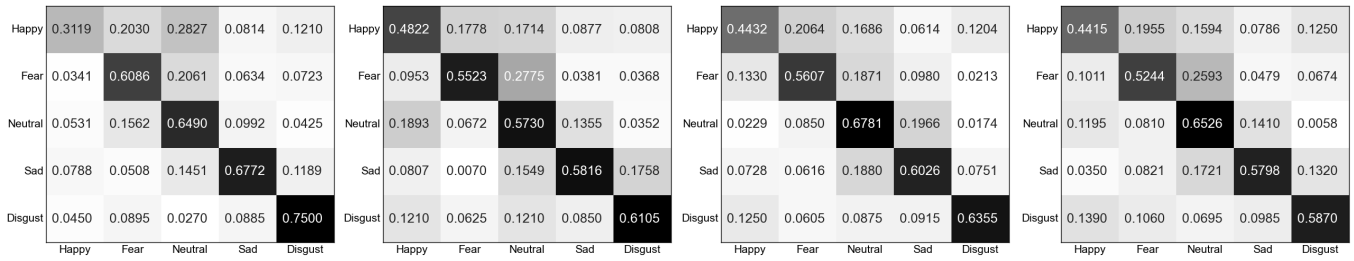

(a) MATL-DC (b) DANN (c) DAN (d) DCORAL

Fig. 5: Confusion matrices of different model settings under cross-subject single-session leave-one-subject-out cross-validation. The Seed-V database contains five emotion categories: happiness, neutral, sadness, disgust and fear. Among them, (a) MATL-DC; (b) DANN; (c) DAN; (d) DCORAL. The horizontal axis represents the predicted labels, while the vertical axis represents the true labels.

model (RF: 72.78%), the performance of the MATL-DC model is improved by 7.43%. Among the deep learning methods, AdaMatch, DANN and Emt-B achieved similar performance with 78.14% and 78.42% and 78.80% , respectively. Compared with the suboptimal model Emt-B, our proposed MATL-DC is improved by 1.41%. Even though the target domain is not visible, MATL-DC still achieve slightly better performance than the model that depends on both the source domain and the target domain. The results on the SEED-IV dataset are shown in TABLE VI. The MATL-DC model achieves the best emotion recognition performance in the SEED-IV database, with an accuracy of 64.51%, which is significantly improved compared with traditional machine learning methods and deep learning methods. Compared with the sub-optimal deep learning model (GCPL: 62.65%), the performance of MATL-DC is improved by 1.72%. The results on the SEED-V dataset are shown in TABLE VII. In the five EEG emotion categories of SEED-V database, MATL-DC achieves 58.39%±08.63% classification performance. DAN and CORAL have similar performance with 54.27% and 54.68%, respectively. Compared with the sub-optimal model CORAL, MATL-DC improved the accuracy by 3.71%.

All these results suggest that the proposed MATL-DC can maintain robust performance independently of target domain data, effectively handling the challenges posed by inter-subject and inter-session variability in EEG-based emotion recognition tasks, which demonstrate the MATL-DC has strong validity and application ability.

F. Confusion Matrix

To qualitatively evaluate the recognition performance of MATL-DC for different emotion categories, we visualize the confusion matrices of MATL-DC on SEED, SEED-IV and SEED-V datasets. Here, the Y-axis represents the True label and the X-axis represents the predicted label.

As shown in Fig.4.(a)∼(d), on the SEED dataset, MATL-DC is similar to the other models, which has the best accuracy in recognizing positive emotions. In addition, MATL-DC has relatively excellent recognition performance, and the recognition accuracy of various emotions is all higher than 82%. In the DCORAL model, the performance discrepancy in identifying positive emotions and negative emotions is 10.4%, while the performance discrepancy in identifying different emotions in MATL-DC is only 4.03%. This indicates that the MATL-DC model has high stability and its performance will not fluctuate greatly, which further demonstrates that the MATL-DC has greatly robustness.

The confusion matrix on the SEED-IV dataset is shown in Fig.4.(e)∼(h). All the participating models performed poorly in recognizing the emotion of happy, while they all performed well in recognizing the other three emotions. When identifying neutral and sad emotions, compared to the suboptimal models DANN (65.96%) and DCORAL (59.56%), the performance of the MATL-DC model was improved by 4.36% and 11.59%, respectively. When identifying fear and happy emotions, the performance of MATL-DC was improved by 14.36% and 2.25% respectively compared with the suboptimal model DAN.

As shown in Fig.5.(a)∼(d), on the SEED-V dataset, the proposed MATL-DC model has weak performance in identifying happy emotions, and is easy to confuse happy emotions with neutral emotions. On the contrary, MATL-DC has the best performance in recognizing fear, sadness and nausea with 60.86%, 67.72% and 75.00%, respectively. Compared with the sub-optimal model, the performance of MATL-DC is improved by 4.79%, 7.46% and 11.45%, respectively.

V. Discussion and Conclusion

A. Visualization of Domain and Class Features

To intuitively understand the influence of the domain and class features extracted by the MATL-DC model and the multi-domain aggregation module, we performed T-SNE visualization of features based on the SEED database in order to clearly understand the evolution of features and prototypes during training.

As shown in Fig.6, we visualize the domain features and domain prototype representation of the MATL-DC model without the multi-domain aggregation module (a)∼(c) and with the multi-domain aggregation module (d)∼(f). Different colors represent different domain features, '$\diamond$' represent the domain prototypes for each domain, and the black '$\times$' represent the target domain features. In (a)∼(c), When without the multi-domain aggregation strategy, too many domain Spaces failed

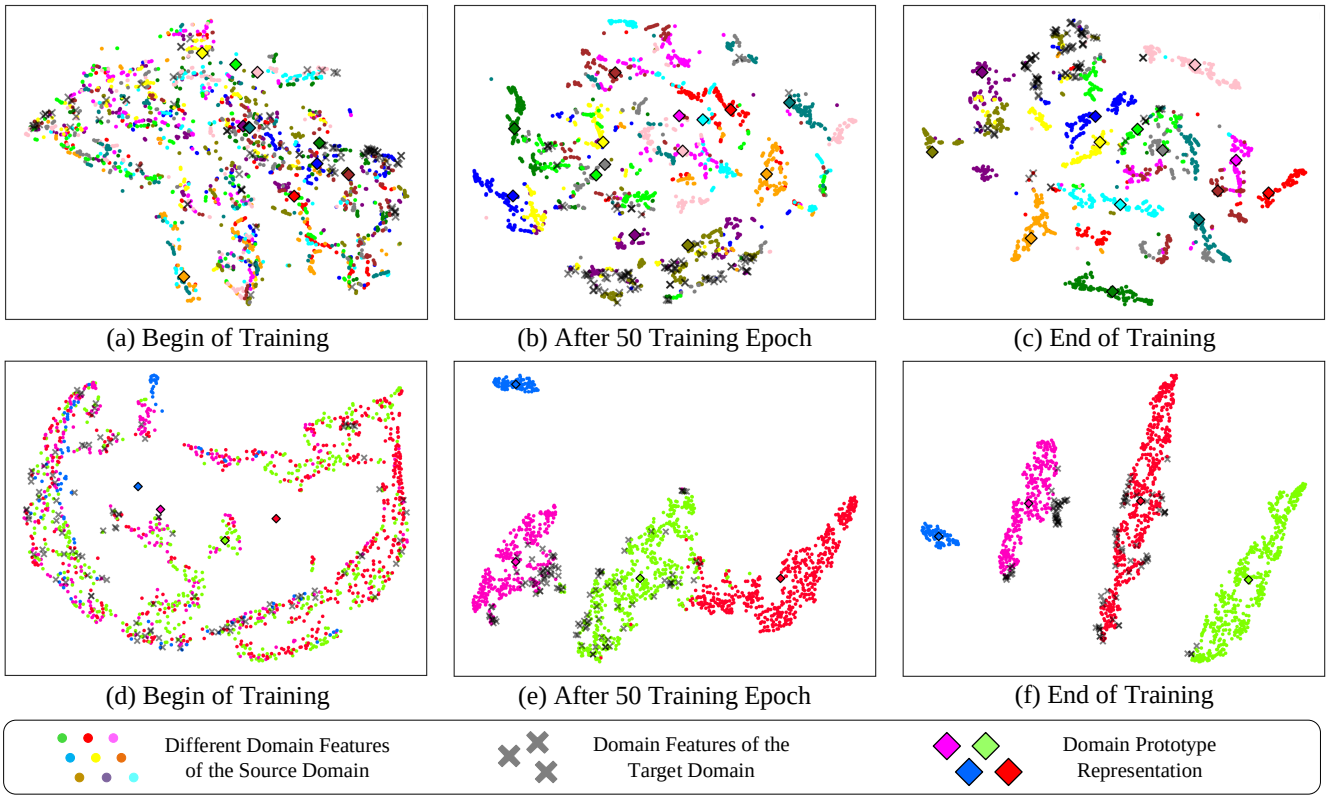

Fig. 6: T-SNE visualizations of domain features and domain prototype representations of the MATL-DC model *without* the Multi-Domain Aggregation module (a)∼(c) and *with* the Multi-Domain Aggregation module (d)∼(f), showing the distribution of domain features at the beginning of training, after 50 training epoch and end of training, respectively. As the model continues to train, the domain features become more and more clustered.

to fully explore the potential correlations between samples and subjects, as well as limited utilization of source domain data. There are no clear boundaries between domain features, and even a certain degree of overlap occurs. In addition, this also leads to an increase in computational cost. Based on the previous assumptions, we believe that EEG samples from different subjects have certain potential connections with multiple domains. Therefore, as shown in (d)∼(f), we aggregate multiple domains into ascertainable superdomains. End of training, the domain features of each superdomain are more compact in the feature space and have clear boundaries with each other, and the domain prototype representations are located at the center of each cluster. At the same time, we can observe that there is a certain imbalance in the feature distribution between different superdomains, which indicates that the commonality of feature distribution among different subjects is different, which leads to different sizes of superdomains.

Further, as shown in Fig.7, we visualize the class feature distribution. With the continuous training of the model, we can obviously observe that the intra-class features are gradually closer, and inter-class features are gradually widened, forming a very clear class feature cluster, which shows the class separability of the model with different class features.

TABLE VIII: Results of ablation experiments with the MATL-DC model, expressed as (Mean-Accuracy%±Standard-Deviation%)

Ablation Strategy	$P_{acc}(\%)$
w/o Domain Prototype	78.95 ± 08.92
w/o Class Disc. Loss in Eq.1	81.62 ± 07.16
w/o Domain Disc. Loss in Eq.2	79.34 ± 08.74
w/o Class & Domain Disc. Loss	78.11 ± 09.24
w/o Multi-Domain Aggregation	80.23 ± 05.12
w/o Adaptive Parameters α in Eq.12	81.54 ± 05.86
w/o Pairwise Learning	76.73 ± 06.62
w/o The Bilinear Trans. Matrix θ in Eq.13	82.94 ± 06.31
w/o Soft Regularization $\mathcal{R}$ in Eq.18	83.65 ± 04.89
MATL-DC	**84.70 ± 04.63**

B. Ablation Experiment

In order to comprehensively evaluate the impact of each module in MATL-DC on the overall performance of the model, we conduct ablation experiments on MATL-DC based on the SEED dataset under the Cross-Subject Single-Session Leave-One-Subject-Out Cross-Validation strategy.

The results of Ablation experiments are shown in TABLE VIII. We remove *domain prototype representation*, and the model performance dropped by 5.75% when using only class

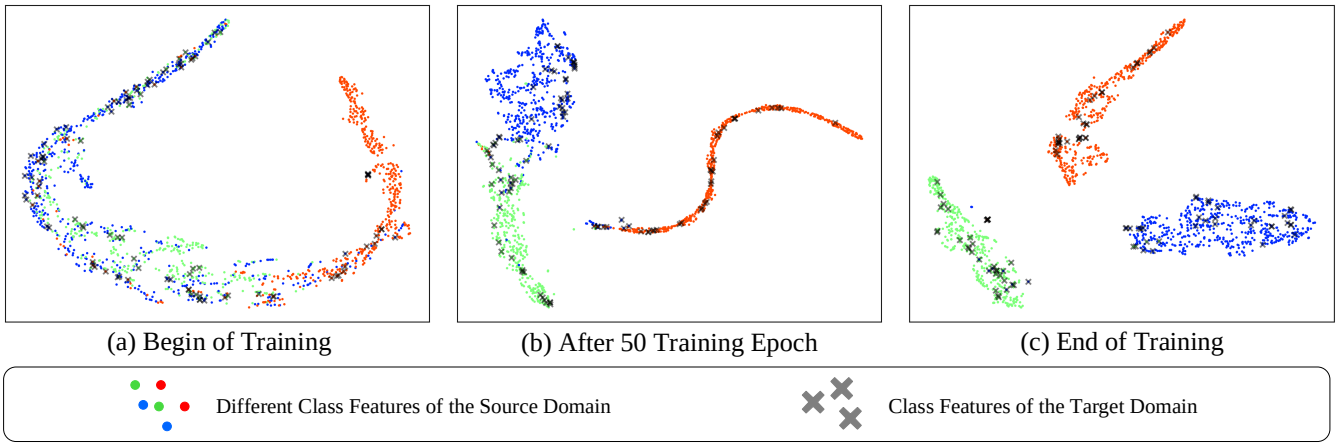

Fig. 7: T-SNE visualizations of source and target class features of the MATL-DC model, showing the distribution of domain features at the (a) beginning of training, (b) after 50 training epoch and (c) end of training, respectively. As the model continues to train, the class features become more and more clustered.

prototypes. This shows that the introduction of domain prototype makes the model have stronger feature representation ability, and then improves the performance of the model. After removing the *class discriminator loss*, the model performance dropped from 84.70% to 81.60%, a decrease of 3.08%. After removing the *domain discriminator loss*, we observed that the model performance dropped by 5.36%. These two experimental results indicate that both domain/class discriminator can enhance the feature decoupling ability of the model. After simultaneously removing the *domain discriminator & class discriminator loss*, the model performance decreased significantly by 6.59%, which indicates that the domain and class discriminator together help to improve the feature extraction ability and significantly improve the recognition performance. After removing *multi-domain aggregation* mechanism, the performance of the model decreases by 4.47%, which indicates that the multi-domain aggregation mechanism fully utilized the potential feature connections among multiple subjects and improves the performance of the model. After removing *adaptive parameter* α, the performance of the model decreases by 3.16%, which indicates that indicates that the adoption of dynamic adaptive update algorithms in prototype computing can enable the model to iterate more stably and avoid possible oscillations. We adopted the traditional pointwise learning strategy instead of *pairwise learning*, and the performance of the model decreased by 7.97%, which indicates that the pairwise learning strategy effectively improves the model performance by converting the classification problem of samples into the similarity problem of sample pairs. After removing the *bilinear transformation matrix* θ, the model performance decreased by 1.76%, which further indicates that θ is beneficial for enhancing the feature representation ability. The MATL-DC performance decreases after removing the *soft regularization* $\mathcal{R}$, which indicates that the introduction of $\mathcal{R}$ is beneficial to avoid redundant feature extraction.

Overall, All these results demonstrate the effectiveness of the individual components in the MATL-DC model and their combined impact on the overall performance.

TABLE IX: Results of the MATL-DC model adding different proportions($\eta\%$) of label noise to the source domain, expressed as (Mean-Accuracy%±Standard-Deviation%). ↓ % denotes the difference between the performances.

Noisy Ratio (η)	Pointwise Learning (%)	Pairwise Learning (%)	Discrepancy (%)
0%	76.73 ± 06.62	84.70 ± 04.63	↓ 07.97
5%	75.89 ± 06.75	83.61 ± 05.28	↓ 07.72
10%	73.45 ± 05.94	83.02 ± 05.06	↓ 09.57
20%	71.84 ± 07.96	82.31 ± 04.94	↓ 10.47
30%	70.04 ± 07.63	81.38 ± 05.68	↓ 11.34
(30%-0%)	↓ 06.69	↓ 03.32	

C. *Effect of Noisy Labels*

We effectively overcame the problem of label noise by pairwise learning strategy. In order to verify the robustness of the model under the pairwise learning and pointwise learning strategies and its dependence on the sample labels, we train the model using the source domain samples with manually added noise. Specifically, We replaced $\eta\%$ of the true labels in the source domain with random noise labels in a controlled manner, and evaluate the model on target domain samples. We set η to 5%, 10%, 20% and 30%. It is worth noting that the sample data of the target domain are completely unseen during training.

As shown in TABLE IX. In the pointwise learning strategy, the model's performance at different values $\eta\%$ is 76.73%, 75.89%, 73.45%, 71.84% and 70.04%, respectively. When the label noise rate η is 30%, the performance of the model decreases by 6.69%, with a significant decline in performance, which indicates that the pointwise learning strategy has limited robustness to label noise, and the model is susceptible to label noise. In the paired learning strategy, when the label noise rate $\eta\%$ gradually increases from 0% to 30%, the performance of the model decreases from 84.70% to 81.38%, and the overall performance decreases only by 3.32%. These results indicate

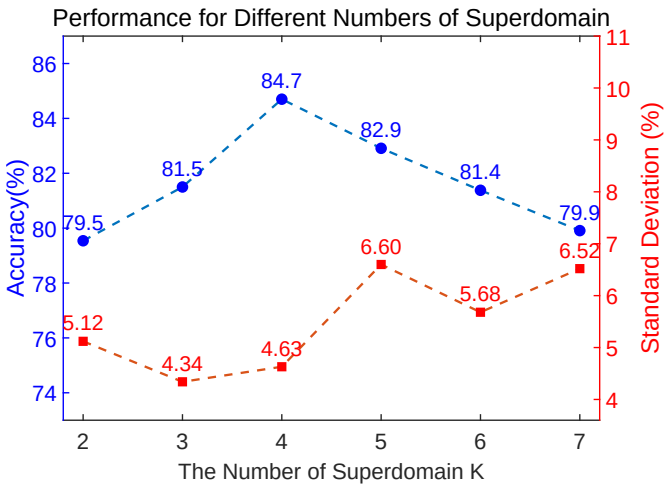

Fig. 8: Performance of the MATL-DC model under different number of aggregates K.

that the pairwise learning strategy has a high tolerance to noisy labels. In addition, we observed that as η continues to increase, the discrepancy in performance between the two strategies of the model gradually widens.

All these results show that the impact of label noise on model performance is limited, and our proposed MATL-DC model has excellent robustness and reliability.

D. Number of Superdomains

To evaluate the relationship between the value of the superdomain number K and the model performance in the multi-domain aggregation mechanism, and to find the most appropriate K, we evaluated the changes in the model performance of MATL-DC under different K.

As shown in Fig.8, the blue vertical axis on the left represents the recognition accuracy of the model, and the red vertical axis on the right represents the standard deviation of the verification result. We gradually increased the value of K from 2 to 7, and the model performance changed significantly. When $K = 4$, the model performance reaches its peak at 84.7%±4.63%. Therefore, considering all factors, we set K to 4 to obtain the optimal model parameters. In addition, we observed that when K is too small, domain features with low similarity in feature distribution are forcibly clustered into the same superdomain, resulting in a decrease in model performance. When K is too large, although the sample features may be slightly discrepancy from the actual domain distribution, if clustering into a new superdomain, the boundary between the superdomains will be unclear or even overlapping, resulting model performance degradation, which is also illustrated by the feature visualization in Fig.6.(c)(f).

E. Conclusion

This work proposes a Multi-domain Aggregation Transfer Learning framework for EEG emotion recognition with Domain-Class prototype (MATL-DC), which breaks through the dependence of traditional transfer learning frameworks on source and target domain. We designed a feature decoupling module to separate domain-class features. And a multi-domain aggregation mechanism was designed to adaptively obtain domain prototype and class prototype representations. In addition, MATL-DC addresses the negative impact of emotional label noise. MATL-DC has achieved advanced performance in several public databases, and provides a potential solution for emotion recognition under unseen target conditions.

ACKNOWLEDGEMENTS

This work was supported in part by the National Natural Science Foundation of China under Grant 62176089, 62276169 and 62201356, in part by the Natural Science Foundation of Hunan Province under Grant 2023JJ20024, in part by the Key Research and Development Project of Hunan Province under Grant 2025QK3008, in part by the Key Project of Xiangjiang Laboratory under Granted 23XJ02006, in part by the STI 2030-Major Projects 2021ZD0200500, in part by the Medical-Engineering Interdisciplinary Research Foundation of Shenzhen University under Grant 2024YG008, in part by the Shenzhen University-Lingnan University Joint Research Programme, and in part by Shenzhen-Hong Kong Institute of Brain Science-Shenzhen Fundamental Research Institutions (2023SHIBS0003).

REFERENCES

[1] D. Schacter, D. Gilbert, and D. Wegner, *Psychology (2nd ed.)*. Annual Review of Neuroscience, Jan 2011.

[2] S. PARADISO, "Affective neuroscience: The foundations of human and animal emotions," *American Journal of Psychiatry*, vol. 159, no. 10, pp. 1805–1805, 2002.

[3] L. Tian, J. D. Moore, and C. Lai, "Recognizing emotions in spoken dialogue with acoustic and lexical cues," in *Proceedings of the 1st ACM SIGCHI International Workshop on Investigating Social Interactions with Artificial Agents*, Nov 2017, p. 45–46.

[4] B. Sun, L. Li, X. Wu, T. Zuo, Y. Chen, G. Zhou, J. He, and X. Zhu, "Combining feature-level and decision-level fusion in a hierarchical classifier for emotion recognition in the wild," *Journal on Multimodal User Interfaces*, vol. 10, p. 125–137, Jun 2016.

[5] Y. Zhao, X. Wang, M. Goubran, T. Whalen, and E. M. Petriu, "Human emotion and cognition recognition from body language of the head using soft computing techniques," *Journal of Ambient Intelligence and Humanized Computing*, vol. 4, no. 1, p. 121–140, Feb 2013.

[6] F. Agrafioti, D. Hatzinakos, and A. K. Anderson, "Ecg pattern analysis for emotion detection," *IEEE Transactions on Affective Computing*, vol. 3, no. 1, pp. 102–115, 2012.

[7] W. Ye, Z. Zhang, F. Teng, M. Zhang, J. Wang, D. Ni, F. Li, P. Xu, and Z. Liang, "Semi-supervised dual-stream self-attentive adversarial graph contrastive learning for cross-subject eeg-based emotion recognition," *IEEE Transactions on Affective Computing*, vol. 16, no. 1, pp. 290–305, 2025.

[8] W. Ye, J. Wang, L. Chen, L. Dai, Z. Sun, and Z. Liang, "Adaptive spatial–temporal aware graph learning for eeg-based emotion recognition," *Cyborg and Bionic Systems*, vol. 6, p. 0088, 2025.

[9] Siddharth, T.-P. Jung, and T. J. Sejnowski, "Utilizing deep learning towards multi-modal bio-sensing and vision-based affective computing," *IEEE Transactions on Affective Computing*, vol. 13, no. 01, pp. 96–107, Jan. 2022.

[10] W. Li, W. Huan, B. Hou, Y. Tian, Z. Zhang, and A. Song, "Can emotion be transferred?—a review on transfer learning for eeg-based emotion recognition," *IEEE Transactions on Cognitive and Developmental Systems*, vol. 14, no. 3, pp. 833–846, 2022.

[11] V. Jayaram, M. Alamgir, Y. Altun, B. Scholkopf, and M. Grosse-Wentrup, "Transfer learning in brain-computer interfaces," *IEEE Computational Intelligence Magazine*, vol. 11, no. 1, pp. 20–31, 2016.

[12] J. Li, S. Qiu, Y.-Y. Shen, C.-L. Liu, and H. He, "Multisource transfer learning for cross-subject eeg emotion recognition," *IEEE Transactions on Cybernetics*, vol. 50, no. 7, pp. 3281–3293, 2020.

[13] H. Cui, A. Liu, X. Zhang, X. Chen, K. Wang, and X. Chen, "Eeg-based emotion recognition using an end-to-end regional-asymmetric convolutional neural network," *Knowledge-Based Systems*, vol. 205, p. 106243, 2020.

[14] P. Zhong, D. Wang, and C. Miao, "Eeg-based emotion recognition using regularized graph neural networks," *IEEE Transactions on Affective Computing*, vol. 13, no. 3, pp. 1290–1301, 2022.

[15] X. Gu, Z. Cao, A. Jolfaei, P. Xu, D. Wu, T.-P. Jung, and C.-T. Lin, "Eeg-based brain-computer interfaces (bcis): A survey of recent studies on signal sensing technologies and computational intelligence approaches and their applications," *IEEE/ACM Transactions on Computational Biology and Bioinformatics*, vol. 18, no. 5, pp. 1645–1666, 2021.

[16] O. Özdenizci, Y. Wang, T. Koike-Akino, and D. Erdoğmuş, "Adversarial deep learning in eeg biometrics," *IEEE Signal Processing Letters*, vol. 26, no. 5, pp. 710–714, 2019.

[17] D. Bethge, P. Hallgarten, T. Grosse-Puppendahl, M. Kari, R. Mikut, A. Schmidt, and O. Özdenizci, "Domain-invariant representation learning from eeg with private encoders," in *IEEE International Conference on Acoustics, Speech and Signal Processing (ICASSP)*, 2022, pp. 1236–1240.

[18] O. Özdenizci, Y. Wang, T. Koike-Akino, and D. Erdoğmuş, "Learning invariant representations from eeg via adversarial inference," *IEEE Access*, vol. 8, pp. 27 074–27 085, 2020.

[19] Y. Yang, Z. Wang, W. Tao, X. Liu, Z. Jia, B. Wang, and F. Wan, "Spectral-spatial attention alignment for multi-source domain adaptation in eeg-based emotion recognition," *IEEE Transactions on Affective Computing*, vol. 15, no. 4, pp. 2012–2024, 2024.

[20] H. Chen, M. Jin, Z. Li, C. Fan, J. Li, and H. He, "Ms-mda: Multisource marginal distribution adaptation for cross-subject and cross-session eeg emotion recognition," *Frontiers in Neuroscience*, vol. 15, p. 778488, 2021.

[21] L.-M. Zhao, X. Yan, and B.-L. Lu, "Plug-and-play domain adaptation for cross-subject eeg-based emotion recognition," *Proceedings of the AAAI Conference on Artificial Intelligence*, p. 863–870, Sep 2022.

[22] R. Paranjape, J. Mahovsky, L. Benedicenti, and Z. Koles, "The electroencephalogram as a biometric," in *Canadian Conference on Electrical and Computer Engineering 2001. Conference Proceedings (Cat. No. 01TH8555)*, vol. 2. IEEE, 2001, pp. 1363–1366.

[23] J. J. Gross and O. P. John, "Revealing feelings: facets of emotional expressivity in self-reports, peer ratings, and behavior," *Journal of personality and social psychology*, vol. 72, no. 2, p. 435, 1997.

[24] H. Bao, T. Shimada, L. Xu, I. Sato, and M. Sugiyama, "Similarity-based classification: Connecting similarity learning to binary classification," *arXiv preprint arXiv:2006.06207*, 2020.

[25] C.-C. Hsu, Y.-X. Zhuang, and C.-Y. Lee, "Deep fake image detection based on pairwise learning," *Applied Sciences*, vol. 10, no. 1, 2020.

[26] M.-K. Kim, M. Kim, E. Oh, and S.-P. Kim, "A review on the computational methods for emotional state estimation from the human eeg," *Computational and mathematical methods in medicine*, vol. 2013, no. 1, p. 573734, 2013.

[27] X.-W. Wang, D. Nie, and B.-L. Lu, *EEG-Based Emotion Recognition Using Frequency Domain Features and Support Vector Machines*. Springer, 2011, p. 734–743.

[28] R.-N. Duan, J.-Y. Zhu, and B.-L. Lu, "Differential entropy feature for eeg-based emotion classification," in *2013 6th International IEEE/EMBS Conference on Neural Engineering (NER)*, Nov 2013.

[29] Z. Mohammadi, J. Frounchi, and M. Amiri, "Wavelet-based emotion recognition system using eeg signal," *Neural Computing and Applications*, vol. 28, p. 1985–1990, 2017.

[30] Y.-H. Liu, C.-T. Wu, Y.-H. Kao, and Y.-T. Chen, "Single-trial eeg-based emotion recognition using kernel eigen-emotion pattern and adaptive support vector machine," in *2013 35th Annual International Conference of the IEEE Engineering in Medicine and Biology Society (EMBC)*, Jul 2013, p. 4306–4309.

[31] S. M. Alarcão and M. J. Fonseca, "Emotions recognition using eeg signals: A survey," *IEEE Transactions on Affective Computing*, vol. 10, no. 3, pp. 374–393, 2019.

[32] Y. Zhou, F. Li, Y. Li, Y. Ji, L. Zhang, Y. Chen, W. Zheng, and G. Shi, "Eeg-based emotion style transfer network for cross-dataset emotion recognition," *arXiv preprint arXiv:2308.05767*, 2023.

[33] Y. Li, W. Zheng, Y. Zong, Z. Cui, T. Zhang, and X. Zhou, "A bi-hemisphere domain adversarial neural network model for eeg emotion recognition," *IEEE Transactions on Affective Computing*, vol. 12, no. 2, pp. 494–504, 2021.

[34] Z. He, Y. Zhong, and J. Pan, "An adversarial discriminative temporal convolutional network for eeg-based cross-domain emotion recognition," *Computers in biology and medicine*, vol. 141, p. 105048, 2022.

[35] J. Li, S. Qiu, C. Du, Y. Wang, and H. He, "Domain adaptation for eeg emotion recognition based on latent representation similarity," *IEEE Transactions on Cognitive and Developmental Systems*, vol. 12, no. 2, pp. 344–353, 2019.

[36] Y. Luo, S.-Y. Zhang, W.-L. Zheng, and B.-L. Lu, *WGAN Domain Adaptation for EEG-Based Emotion Recognition*. springer, Jan 2018, p. 275–286.

[37] C.-L. Liu and M. Nakagawa, "Evaluation of prototype learning algorithms for nearest-neighbor classifier in application to handwritten character recognition," *Pattern Recognition*, p. 601–615, Mar 2001.

[38] Y. Wang, S. Qiu, C. Zhao, W. Yang, J. Li, X. Ma, and H. He, "Eeg-based emotion recognition with prototype-based data representation," in *2019 41st Annual International Conference of the IEEE Engineering in Medicine and Biology Society (EMBC)*, Jul 2019.

[39] R. Zhou, Z. Zhang, H. Fu, L. Zhang, L. Li, G. Huang, F. Li, X. Yang, Y. Dong, Y.-T. Zhang, and Z. Liang, "Pr-pl: A novel prototypical representation based pairwise learning framework for emotion recognition using eeg signals," *IEEE Transactions on Affective Computing*, vol. 15, no. 2, pp. 657–670, 2024.

[40] Y. Wang, S. Qiu, X. Ma, and H. He, "A prototype-based spd matrix network for domain adaptation eeg emotion recognition," *Pattern Recognition*, vol. 110, p. 107626, 2021.

[41] Y. Guo, C. Tang, H. Wu, and B. Chen, "Gnn-based multi-source domain prototype representation for cross-subject eeg emotion recognition," *Neurocomputing*, vol. 609, p. 128445, 2024.

[42] H. Zhang, Y.-F. Zhang, W. Liu, A. Weller, B. Schölkopf, and E. P. Xing, "Towards principled disentanglement for domain generalization," in *Proceedings of the IEEE/CVF Conference on Computer Vision and Pattern Recognition (CVPR)*, June 2022, pp. 8024–8034.

[43] R. Cai, Z. Li, P. Wei, J. Qiao, K. Zhang, and Z. Hao, "Learning disentangled semantic representation for domain adaptation," in *IJCAI: proceedings of the conference*, vol. 2019, 2019, p. 2060.

[44] X. Peng, Z. Huang, X. Sun, and K. Saenko, "Domain agnostic learning with disentangled representations," in *Proceedings of the 36th International Conference on Machine Learning*, ser. Proceedings of Machine Learning Research, vol. 97, 2019, pp. 5102–5112.

[45] W.-L. Zheng and B.-L. Lu, "Investigating critical frequency bands and channels for eeg-based emotion recognition with deep neural networks," *IEEE Transactions on Autonomous Mental Development*, vol. 7, no. 3, pp. 162–175, 2015.

[46] W.-L. Zheng, W. Liu, Y. Lu, B.-L. Lu, and A. Cichocki, "Emotionmeter: A multimodal framework for recognizing human emotions," *IEEE Transactions on Cybernetics*, vol. 49, no. 3, pp. 1110–1122, 2019.

[47] W. Liu, J.-L. Qiu, W.-L. Zheng, and B.-L. Lu, "Comparing recognition performance and robustness of multimodal deep learning models for multimodal emotion recognition," *IEEE Transactions on Cognitive and Developmental Systems*, vol. 14, no. 2, pp. 715–729, 2021.

[48] R.-N. Duan, J.-Y. Zhu, and B.-L. Lu, "Differential entropy feature for eeg-based emotion classification," in *2013 6th International IEEE/EMBS Conference on Neural Engineering (NER)*, 2013, pp. 81–84.

[49] L.-C. Shi and B.-L. Lu, "Off-line and on-line vigilance estimation based on linear dynamical system and manifold learning," in *2010 Annual International Conference of the IEEE Engineering in Medicine and Biology*, 2010, pp. 6587–6590.

[50] D. Coomans and D. L. Massart, "Alternative k-nearest neighbour rules in supervised pattern recognition: Part 1. k-nearest neighbour classification by using alternative voting rules," *Analytica Chimica Acta*, vol. 136, pp. 15–27, 1982.

[51] S. Mika, B. Schölkopf, A. Smola, K.-R. Müller, M. Scholz, and G. Rätsch, "Kernel pca and de-noising in feature spaces," in *Proceedings of the 12th International Conference on Neural Information Processing Systems*, ser. NIPS'98. Cambridge, MA, USA: MIT Press, 1998, p. 536–542.

[52] J. A. Suykens and J. Vandewalle, "Least squares support vector machine classifiers," *Neural processing letters*, vol. 9, no. 3, pp. 293–300, 1999.

[53] B. Fernando, A. Habrard, M. Sebban, and T. Tuytelaars, "Unsupervised visual domain adaptation using subspace alignment," in *2013 IEEE International Conference on Computer Vision*, 2013, pp. 2960–2967.

[54] S. J. Pan, I. W. Tsang, J. T. Kwok, and Q. Yang, "Domain adaptation via transfer component analysis," *IEEE Transactions on Neural Networks*, vol. 22, no. 2, pp. 199–210, 2011.

[55] B. Sun, J. Feng, and K. Saenko, "Return of frustratingly easy domain adaptation," in *Proceedings of the Thirtieth AAAI Conference on Artificial Intelligence*. AAAI Press, 2016, p. 2058–2065.

[56] B. Gong, Y. Shi, F. Sha, and K. Grauman, "Geodesic flow kernel for unsupervised domain adaptation," in *IEEE Conference on Computer Vision and Pattern Recognition*, 2012, pp. 2066–2073.

[57] L. Breiman, "Random forests," *Machine learning*, vol. 45, pp. 5–32, 2001.

[58] H. Li, Y.-M. Jin, W.-L. Zheng, and B.-L. Lu, "Cross-subject emotion recognition using deep adaptation networks," in *Neural Information Processing*. Cham: Springer International Publishing, 2018, pp. 403–413.

[59] Y. Ganin, E. Ustinova, H. Ajakan, P. Germain, H. Larochelle, F. Laviolette, M. Marchand, and V. Lempitsky, "Domain-adversarial training of neural networks," *J. Mach. Learn. Res.*, vol. 17, no. 1, p. 2096–2030, 2016.

[60] E. Tzeng, J. Hoffman, N. Zhang, K. Saenko, and T. Darrell, "Deep domain confusion: Maximizing for domain invariance," *ArXiv*, vol. abs/1412.3474, 2014.

[61] B. Sun and K. Saenko, "Deep coral: Correlation alignment for deep domain adaptation," in *Computer Vision – ECCV 2016 Workshops*, G. Hua and H. Jégou, Eds. Cham: Springer International Publishing, 2016, pp. 443–450.

[62] T. Song, W. Zheng, P. Song, and Z. Cui, "Eeg emotion recognition using dynamical graph convolutional neural networks," *IEEE Transactions on Affective Computing*, vol. 11, no. 3, pp. 532–541, 2018.

[63] D. Sejdinovic, B. Sriperumbudur, A. Gretton, and K. Fukumizu, "Equivalence of distance-based and rkhs-based statistics in hypothesis testing," *Annals of Stats*, vol. 41, no. 5, pp. 2263–2291, 2013.

[64] Y. Ding, N. Robinson, S. Zhang, Q. Zeng, and C. Guan, "Tsception: Capturing temporal dynamics and spatial asymmetry from eeg for emotion recognition," *IEEE Transactions on Affective Computing*, vol. 14, no. 3, pp. 2238–2250, 2022.

[65] W. Zhang, F. Wang, Y. Jiang, Z. Xu, S. Wu, and Y. Zhang, "Cross-subject eeg-based emotion recognition with deep domain confusion," in *Intelligent Robotics and Applications: 12th International Conference, ICIRA 2019, Shenyang, China, August 8–11, 2019, Proceedings, Part I 12*. Springer, 2019, pp. 558–570.

[66] D. Berthelot, R. Roelofs, K. Sohn, N. Carlini, and A. Kurakin, "Adamatch: A unified approach to semi-supervised learning and domain adaptation," in *International Conference on Learning Representations*, 2022. [Online]. Available: https://openreview.net/forum?id=Q5uh1Nvv5dm

[67] Y. Ding, C. Tong, S. Zhang, M. Jiang, Y. Li, K. J. Lim, and C. Guan, "Emt: A novel transformer for generalized cross-subject eeg emotion recognition," *IEEE Transactions on Neural Networks and Learning Systems*, vol. 36, no. 6, pp. 10 381–10 393, 2025.

[68] T. Song, S. Liu, W. Zheng, Y. Zong, and Z. Cui, "Instance-adaptive graph for eeg emotion recognition," in *Proceedings of the AAAI Conference on Artificial Intelligence*, vol. 34, no. 03, 2020, pp. 2701–2708.

[69] Y. Xu, Y. Du, L. Li, H. Lai, J. Zou, T. Zhou, L. Xiao, L. Liu, and P. Ma, "Amdet: Attention based multiple dimensions eeg transformer for emotion recognition," *IEEE Transactions on Affective Computing*, vol. 15, no. 3, pp. 1067–1077, 2023.

[70] T. Zhang, X. Wang, X. Xu, and C. L. P. Chen, "Gcb-net: Graph convolutional broad network and its application in emotion recognition," *IEEE Transactions on Affective Computing*, vol. 13, no. 1, pp. 379–388, 2022.

[71] W. Li, L. Fan, S. Shao, and A. Song, "Generalized contrastive partial label learning for cross-subject eeg-based emotion recognition," *IEEE Transactions on Instrumentation and Measurement*, vol. 73, pp. 1–11, 2024.

[72] T. Song, W. Zheng, C. Lu, Y. Zong, X. Zhang, and Z. Cui, "Mped: A multi-modal physiological emotion database for discrete emotion recognition," *IEEE Access*, vol. 7, pp. 12 177–12 191, 2019.

[73] E. Eldele, M. Ragab, Z. Chen, M. Wu, C.-K. Kwoh, X. Li, and C. Guan, "Adast: Attentive cross-domain eeg-based sleep staging framework with iterative self-training," *IEEE Transactions on Emerging Topics in Computational Intelligence*, vol. 7, no. 1, pp. 210–221, 2022.

[74] M. Jiménez-Guarneros and G. Fuentes-Pineda, "Learning a robust unified domain adaptation framework for cross-subject eeg-based emotion recognition," *Biomedical Signal Processing and Control*, vol. 86, p. 105138, 2023.